The First Assembly of a Nest-Shaped Heterothiometallic Cluster and a Polyoxometalate Anion − Synthesis, Characterization, and Strong Third-Order Nonlinear Optical Response

Chi Zhang,*[a,b,c] Yinglin Song,[a] Fritz E. Kühn,*[b] Yan Xu,[d] Xinquan Xin,[d] Hoongkun Fun,[a,b,c] and Wolfgang A. Herrmann*[b]

Keywords: Polyoxometalates / Transition metals / Cluster compounds / Nonlinear optics

Two heterothiometallic cluster compounds $[MOS_3Cu_3(4\text{-pic})_6]\cdot 0.5[M_2O_7]$ (M = Mo **1**, W **2**) having a cationic cluster skeleton and a polyoxometalate cluster anion, as well as two other clusters $[MOS_3Cu_3(4\text{-pic})_6]\cdot[BF_4]$ (M = Mo **3**, W **4**) have been synthesized for nonlinear optics studies. Single-crystal X-ray diffraction data show that cluster **1** adopts a very interesting arrangement with a cationic nest-shaped cluster skeleton and a polyoxomolybdenum cluster anion. This is the first time that such a skeleton has been found for an Mo/S/Cu heterothiometallic cluster compound and it represents a distinct structural type as compared to the analogous nest-shaped clusters seen with a neutral or an anionic skeleton. The nonlinear optical properties of these four clusters have been investigated with an 8 ns pulsed laser at 532 nm, and optical self-focusing effects have been observed. Clusters **1** and **2** with the polyoxometalate cluster anion exhibit stronger third-order nonlinear optical absorption than clusters **3** and **4** having only a pseudo-halogen group as the anion, which can be attributed to skeletal differences. Clusters **1** and **2** also exhibit very large optical limiting effects toward the ns incident pulsed laser as compared with clusters **3** and **4** and other shaped clusters with the same skeleton factors studied previously. This demonstrates the influence of the cluster skeleton on the nonlinear optical performance.

Introduction

The chemistry of transition metal sulfur clusters has attracted considerable attention[1] and represents an important and active area of research concerning advanced materials, biological processes, and catalytic reactions.[2−4] This is because these clusters possess interesting electronic, biological, optical, structural, and catalytic properties and show promising potential as biological models of some nitrogenases or various other metalloenzymes,[4a,5] as active centers relevant to some industrial catalytic processes,[1a] and as precursor molecules of optically functional materials for optical limiting applications and optical signal detection techniques.[2] Currently, the tremendous interest in these clusters is mainly focused on the search for better materials with third-order nonlinear optical (NLO) properties and superior optical limiting (OL) effects, not only for applications in protecting optical sensors and human eyes from high-intensity laser hazards, but also for their utilization in optical communication, optical signal processing and transmission, optical data acquisition and storage, optical computing, and optic-electronic modulation.

The ongoing research and development in this promising field shows that, in contrast to the other most frequently mentioned NLO materials, such as phthalocyanine or fullerene C_{60} and derivatives thereof,[6,7] these clusters possess the combined advantages of both organic molecules and inorganic compounds: large modifiable structures and structures containing many heavy metal atoms. One of the most important and promising features of these heterothiometallic clusters is the possibility of modifying and eventually optimizing the building blocks through subtle modifications at the molecular level. Thus, all of the structural units, terminal ligands, skeletal elements, and constituent components can be altered just like organic molecules so that the NLO properties can be adjusted through structural manipulation. On the other hand, the incorporation of heavy metal atoms may introduce more sublevels into the energy hierarchy as compared to organic molecules with the

[a] Department of Applied Physics,
Harbin Institute of Technology,
Harbin 150001, P. R. China
[b] Anorganisch-Chemisches Institut der Technischen Universität München,
Lichtenbergstrasse 4, 85747 Garching bei München, Germany
[c] Department of Chemistry, University of Kansas,
Lawrence, Kansas 66045, USA
[d] State Key Laboratory of Coordination Chemistry,
Department of Chemistry, Nanjing University,
Nanjing 210093, P. R. China
[e] X-ray Crystallography Unit, School of Physics,
Universiti Sains Malaysia 11800, USM,
Penang, Malaysia

  1434−1948/02/0101−0055 $ 17.50+.50/0

same number of skeleton atoms. This permits more allowed electron transitions, thereby leading to larger NLO effects, especially those beneficial to NLO applications. Our studies on these clusters have demonstrated that, unlike some traditional NLO materials, their skeletons and constituent elements have a considerable influence on their NLO performances, which results in the Mo(W)/S/Cu(Ag) clusters exhibiting rather diverse combinations of NLO effects. Clusters having a cubane-like shape,[2a,8] a half-open cubane-like shape,[2b,9] and a hexagonal prism-shape[10] show strong nonlinear absorption. Strong nonlinear refraction effects are exhibited by some nest-shaped,[11] twin-nest-shaped,[12] and butterfly-shaped clusters.[13] The previously described twenty-nuclear supra-cage-shaped cluster[2d] possesses very large nonlinear susceptibility, while hexagonal prism-shaped clusters,[10] pentanuclear planar "open" clusters,[14] and cluster polymers[15] exhibit large optical limiting properties. Nevertheless, there remains a challenge to develop optically functional materials with strong third-order NLO properties and superior OL effects, and to establish the general relationships between the cluster molecular structures and their NLO performances.

In our systematic efforts to investigate the possibilities of controlling the size and composition of the cluster skeletons and their third-order NLO properties, including the OL effects, as well as the coordination chemistry of thiometalates with Lewis-base adducts through modification of their backbone, we describe herein the synthesis of a series of nest-shaped clusters **1**−**4** by ligand-redistribution reactions, and report the characterization of their structures by X-ray crystallography. To our surprise, the unexpected products, clusters **1** and **2**, adopt a very interesting arrangement with a cationic nest-shaped cluster skeleton and a polyoxometalate cluster anion. This is the first time that such a skeleton has been found for an Mo/S/Cu(Ag) heterothiometallic cluster compound. The results of *Z*-scan experiments show that these clusters possess strong NLO absorptive abilities and effective optical self-focusing behavior, which are simulated by excited-state absorption theory. Large optical limiting effects of this series of clusters are observed in the OL measurements. The third-order nonlinear optical susceptibilities $\chi^{(3)}$ and the third-order nonlinear hyperpolarizabilities γ of these clusters are also reported.

Results and Discussion

Synthetic Reactions

The cationic cluster skeleton $[MOS_3Cu_3(4\text{-pic})_6]^+$ (M = Mo, W; 4-pic = 4-picoline) present in clusters **1**−**4** was straightforwardly prepared in two steps by a ligand-redistribution reaction. In the first step, the copper complex bearing mixed ligands was pre-synthesized as an intermediate, which did not have to be isolated from the reaction system. In the present case, the starting material CuX [X = Cl^-, $(CH_3CN)_4BF_4^-$] was treated with 4-picoline, which served as both the reaction solvent and the σ-donor ligand. Since 4-pic exhibits a strong super-conjugation effect from the methyl group to the pyridine ring, it can be expected to show a high tendency to coordinate to Cu atoms. The gradual dissolution of CuX with the formation of a light-yellow solution were consistent with the formation of the intermediate product, i.e. the Lewis-base adduct $CuX(4\text{-pic})_3$.[16] Then the synthon thiometalate $[MOS_3]^{2-}$ was added to the reaction system as a bidentate ligand. The solution immediately turned from light-yellow to black-red (or orange-red) in color, which suggested that the target cluster compounds had been formed. Since the sequence of some Cu^I-philic ligands of Mo(W)/S/Cu(Ag) compounds can be regarded as $S^{2-} >$ (py, PPh_3) $> X^-$ (X = Cl, Br, I, CN), the former ligands can substitute part or all of the latter ligands, while the required coordination number of copper is not more than four. Two bonds of $CuX(4\text{-pic})_3$ were broken by the attack of the S^{2-} of the $[MOS_3]^{2-}$ moiety and in forming the final cationic cluster skeleton.

At the stage of forming the final cluster molecules, the BF_4^- anion in the reaction systems of clusters **3** and **4** can help to achieve a charge balance with the cationic cluster skeleton $[MOS_3Cu_3(4\text{-pic})_6]^+$ leading to formation and precipitation of the clusters $[MOS_3Cu_3(4\text{-pic})_6]\cdot[BF_4]$ (M = Mo **3**, W **4**) as expected (Scheme 1). To our surprise, the same does not take place in the reactions leading to the formation of clusters **1** and **2**. This is due to the fact that the expected target clusters $[MOS_3Cu_3(4\text{-pic})_6]\cdot Cl$ were not formed in the same way. These target clusters were to have been prepared to explore the relationship between the constituent components of the clusters and their NLO properties through comparing the isomorphous clusters with the same cationic cluster skeleton and different anions. Previous work has shown that large cations of appropriate size may combine with the anionic cluster skeletons through either charge-transfer or other non-bonding interactions.[17] In such a reaction system, the oxophilic Ca^{2+}, La^{3+}, and Nd^{3+} cations may be coordinated by the oxygen atoms of DMSO or DMF to form the larger bivalent and trivalent complex cations $[M(DMSO)_x]^{n+}$ or $[M(DMF)_x]^{n+}$ (M = Ca, La, Nd; x = 6, 8; n = 2, 3). These complex cations can induce the cluster anions in the solution to assemble into some special structural types of heterothiometallic clusters. In the present reaction systems involving clusters **1** and **2**, we assume that the crystallizing procedure, not being performed in an oxygen- and moisture-free environment, results in the transformation of excess $[MOS_3]^{2-}$ into $[M_2O_7]^{2-}$ (M = Mo, W) due to exposure to oxygen and atmospheric moisture. The polyoxometalate anion $[M_2O_7]^{2-}$, being larger than the Cl^- anion, is much more effective in precipitating the cationic cluster skeletons. Even

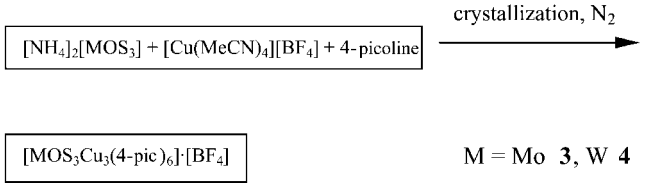

Scheme 1

if the clusters $[MOS_3Cu_3(4\text{-pic})_6]\cdot Cl$ have already formed, the small Cl^- anion can still be easily displaced by $[M_2O_7]^{2-}$. Since the polyoxometalate anion $[M_2O_7]^{2-}$ with the larger, more suitable size can stabilize an appropriately sized cation, the original cluster cations $[MOS_3Cu_3(4\text{-pic})_6]^+$ tend to combine with this large polyoxometalate anion $[M_2O_7]^{2-}$ by the assembly reaction in solution, finally crystallizing from the solution in the form of the interesting cluster skeleton with a cationic nest-shaped cluster skeleton and a polyoxometalate cluster anion (Scheme 2).

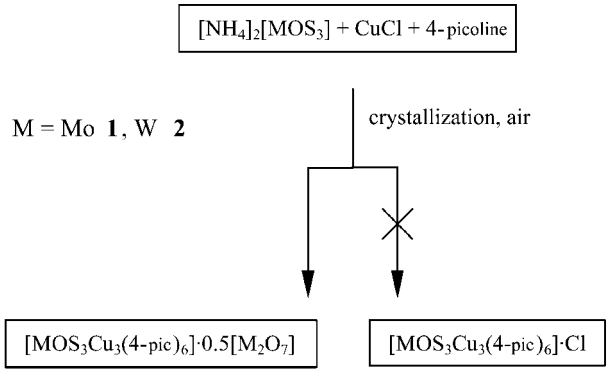

Scheme 2

Structural Description

The crystal structures of these clusters $[MOS_3Cu_3(4\text{-pic})_6]\cdot L$ (M = Mo, W; L = 0.5 M_2O_7, BF_4) reveal a nest-shaped cluster cation and a polyoxometalate cluster anion in the case of **1**, or a pseudo halogen group BF_4^- anion in the case of **4**. To the best of our knowledge, the nest-shaped clusters always adopt the configuration of a neutral skeleton, e.g. $[MOS_3Cu_3I(py)_5]$,[11b] or an anionic skeleton, e.g. $[Bu_4N]_2[MOS_3Cu_3BrCl_2]$[11a] or $[PPh_4]_2[MOS_3(CuCl)_3]$[18] (M = Mo, W). This is the first time that clusters such as **1**, with a cationic nest-shaped cluster skeleton and a polyoxometalate cluster anion, have been found for Mo/S/Cu(Ag) systems and they show a surprising difference in comparison with their nest-shaped cluster analogues. ORTEP plots of clusters **1** and **4** are shown in Figures 1 and 2. Selected

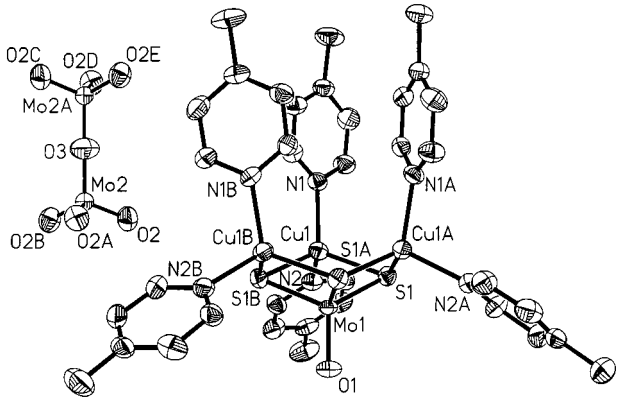

Figure 1. A perspective view of the structure of cluster $[MoOS_3Cu_3(4\text{-pic})_6]\cdot 0.5[Mo_2O_7]$ (**1**)

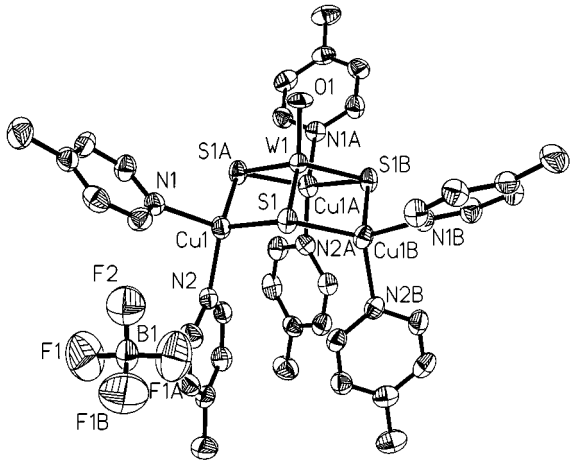

Figure 2. A perspective view of the structure of cluster $[WOS_3Cu_3(4\text{-pic})_6]\cdot[BF_4]$ (**4**)

bond lengths and angles are listed in Tables 1 and 2. Since the structures of the $[MOS_3Cu_3(4\text{-pic})_6]^+$ cation in clusters **1** and **4** are isomorphous, only the structure of cluster **1** is described in detail.

The cationic skeleton of **1**, with an $MoOS_3Cu_3$ aggregate, displays a nest-shaped structure. The central Mo atom is tetrahedrally coordinated by three S atoms and one O atom. The Mo(1)−O(1) bond length of 1.699(8) Å is characteristic of a double bond, while the three equivalent Mo−S bond lengths of 2.2692(17) Å are in the typical range for single bonds. Compared to the free $[MoOS_3]^{2-}$ ion, the $MoOS_3$ fragment adopts an ideal crystallographic C_3 symmetry at 0.3333, 0.3333, z axis through the Mo(1) atom and the O(1) atom, with three equal S−Mo−S bond angles [107.78(5)°]. In addition, weak interactions exist between the Mo atom and the three Cu atoms, while the Mo−Cu distances [2.6879(9) Å] in cluster **1** are slightly shorter than those in $[MoCu_3OS_3(PPh_3)_3\{S_2P(OBu)_2\}]$ [2.739(3) Å][19] and $[MoCu_3OS_3(PPh_3)_3(CH_3COO)]$ [2.710(1) Å].[20] The three Cu atoms exhibit the same coordination mode. Each adopts a distorted tetrahedral geometry and is coordinated by two μ_3-S atoms and two 4-pic ligands, forming three almost equivalent $CuS_2(4\text{-pic})_2$ units. These three $CuS_2(4\text{-pic})_2$ units are joined by a central Mo atom through three pairs of S−S edges, thereby forming the skeleton of the cation $[MOS_3Cu_3(4\text{-pic})_6]^+$. Since they have similar coordination environments, there is no obvious difference between Cu(1), Cu(1A), and Cu(1B). The Cu(1)−S(1) bond length [2.2777(19) Å] is almost identical to the Cu(1)−S(1)($-x + y + 1, -x + 3, z$) [2.2789(18) Å] and S(1)−Cu(1)($-y + 3, x - y + 2, z$) bond lengths [2.2789(18) Å], but the Cu(1)−N(1) distance [2.059(6) Å] is a little shorter than the Cu(1)−N(2) distance [2.107(6) Å]. On the other hand, the average Cu−S bond length [2.2785(18) Å] in cluster **1** is greater than that in its anionic analogue $[Bu_4N]_2[MoOS_3Cu_3BrCl_2]$ [2.238(3) Å] and is akin to that in its neutral analogue $[MoOS_3Cu_3I(py)_5]$ [2.288(5) Å]. This may be attributed to the fact that in cluster **1** and $[MoOS_3Cu_3I(py)_5]$ there is a strong super-conjugation effect in the pyridine

Table 1. Selected bond lengths [Å] and angles [°] for the cluster $[MoOS_3Cu_3(4\text{-pic})_6]\cdot 0.5[Mo_2O_7]$ (1). − Symmetry transformations used to generate equivalent atoms: #1: $-x + y + 1, -x + 3, z$; #2: $-y + 3, x - y + 2, z$; #3: $-y + 1, x - y + 2, z$; #4: $-x + y - 1, -x + 1, z$; #5: $-x, -y + 2, -z$

Mo(1)−O(1)	1.699(8)	Mo(2)−O(2)	1.705(7)
Mo(1)−S(1)	2.2692(17)	Mo(2)−O(2)#3	1.705(7)
Mo(1)−S(1)#1	2.2692(17)	Mo(2)−O(2)#4	1.705(7)
Mo(1)−S(1)#2	2.2692(17)	Mo(2)−O(3)	1.8557(13)
Mo(1)−Cu(1)	2.6879(9)	O(3)−Mo(2)#5	1.8557(13)
Mo(1)−Cu(1)#1	2.6879(9)	Cu(1)−S(1)	2.2777(19)
Mo(1)−Cu(1)#2	2.6879(9)	Cu(1)−S(1)#1	2.2789(18)
Cu(1)−N(1)	2.059(6)	S(1)−Cu(1)#2	2.2789(18)
Cu(1)−N(2)	2.107(6)		
O(1)−Mo(1)−S(1)	111.12(5)	O(2)#3−Mo(2)−O(3)	110.8(3)
O(1)−Mo(1)−S(1)#1	111.12(5)	O(2)−Mo(2)−O(3)	110.8(3)
O(1)−Mo(1)−S(1)#2	111.12(5)	O(2)#4−Mo(2)−O(3)	110.8(3)
S(1)#1−Mo(1)−S(1)	107.78(5)	Mo(2)−O(3)−Mo(2)#5	180.0
S(1)#1−Mo(1)−S(1)#2	107.78(5)	Cu(1)−S(1)−Cu(1)#2	112.93(8)
S(1)#2−Mo(1)−S(1)	107.78(5)	Mo(1)−S(1)−Cu(1)	72.48(5)
O(2)#3−Mo(2)−O(2)	108.1(3)	Mo(1)−S(1)−Cu(1)#2	72.45(5)
O(2)#3−Mo(2)−O(2)#4	108.1(3)	S(1)−Cu(1)−S(1)#1	107.15(8)
O(2)−Mo(2)−O(2)#4	108.1(3)	N(1)−Cu(1)−N(2)	105.3(2)

Table 2. Selected bond lengths [Å] and angles [°] for the cluster $[WOS_3Cu_3(4\text{-pic})_6]\cdot[BF_4]$ (**4**). − Symmetry transformations used to generate equivalent atoms: #1: $-x + y, -x + 1, z$; #2: $-y + 1, x - y + 1, z$; #3: $-x + y, -x, z$; #4: $-y, x - y, z$

W(1)−O(1)	1.772(8)	Cu(1)−S(1)	2.303(2)
W(1)−S(1)	2.2568(19)	S(1)−Cu(1)#1	2.287(2)
W(1)−S(1)#1	2.2568(19)	Cu(1)−S(1)#2	2.287(2)
W(1)−S(1)#2	2.2568(19)	Cu(1)−N(1)	2.098(7)
W(1)−Cu(1)	2.7037(10)	Cu(1)−N(2)	2.029(7)
W(1)−Cu(1)#1	2.7037(10)	F(1)−B(1)	1.308(6)
W(1)−Cu(1)#2	2.7037(11)	F(2)−B(1)	1.316(7)
O(1)−W(1)−S(1)	110.56(5)	N(2)−Cu(1)−N(1)	106.2(3)
O(1)−W(1)−S(1)#1	110.56(5)	S(1)#2−Cu(1)−S(1)	105.77(10)
O(1)−W(1)−S(1)#2	110.56(5)	N(2)−Cu(1)−S(1)	112.62(19)
S(1)−W(1)−S(1)#2	108.36(6)	N(1)−Cu(1)−S(1)#2	108.33(18)
S(1)#1−W(1)−S(1)	108.36(6)	N(1)−Cu(1)−S(1)	106.62(19)
S(1)#1−W(1)−S(1)#2	108.36(6)	N(2)−Cu(1)−S(1)#2	116.81(19)
W(1)−S(1)−Cu(1)	72.72(6)	F(1)−B(1)−F(2)	106.2(7)
W(1)−S(1)−Cu(1)#1	73.03(6)	F(1)#3−B(1)−F(1)#4	112.5(6)
Cu(1)#1−S(1)−Cu(1)	113.99(9)	F(1)#4−B(1)−F(2)	106.2(7)

ring that may result in 4-pic or py showing a high tendency to coordinate to a Cu atom, while the coordination between the Cu atom and the S atoms is weakened accordingly.

The unexpected polyoxometalate dianion $[Mo_2O_7]^{2-}$ formed in the present case originated from the adventitious introduction of air during the crystallization period. The dianion possesses a strict crystallographic C_2 symmetry, in which two MoO_4 tetrahedra share a vertex. The two equivalent MoO_3 moieties in the $[Mo_2O_7]^{2-}$ anion are oriented essentially perpendicularly to their respective Mo(2)−O(3) bonds in an almost eclipsed arrangement. All three independent Mo(2)−O(2) bond lengths are equal [1.705(7) Å] and are slightly longer than the Mo(1)−O(1) bond lengths, this being characteristic of a double bond, while the Mo(2)−O(3) bond lengths [1.8557(13) Å] are in the typical range for single bonds. All six independent O(2)−Mo(2)−O(2)($-x + y - 1, -x + 1, z$) bond angles are the same [108.1(3)°] and are clearly smaller than the O(1)−Mo(1)−S(1) and O(2)−Mo(2)−O(3) bond angles. It is interesting and noteworthy that the O(1)−Mo(1)−S(1) [111.12(5)°] and O(2)−Mo(2)−O(3) [110.8(3)°] bond angles are in the same range, which may be attributed to the Mo(2)−O(3) bond length being typical of a single bond, like the Mo(1)−S single bond. It is also noteworthy that the $[Mo_2O_7]^{2-}$ anion shows a perfectly straight Mo−O−Mo axis in the present case with the Mo(2)−O(3)−Mo(2)($-x, -y + 2, -z$) bond angle being equal to 180.0°, which is clearly different from that described previously [Mo−O−Mo angle 153.6(5)°].[21]

Spectral Characterization

The IR spectra of the $[MOS_3Cu_3(4\text{-pic})_6]\cdot L$ clusters (M = Mo, W; L = 0.5 M_2O_7, BF_4) exhibit strong characteristic bands at 436 cm^{-1} (**1**), 428 cm^{-1} (**2**), 437 cm^{-1} (**3**), and 428 cm^{-1} (**4**) attributable to the μ_3-S stretching vibration, while very strong absorptions at 908 cm^{-1} (**1**), 925 cm^{-1} (**2**), 910 cm^{-1} (**3**), and 924 cm^{-1} (**4**) can be attributed to the characteristic $\nu(M-O_t)$ vibration of the bridging MOS_3 group. In addition, due to the presence of $[M_2O_7]^{2-}$ anions, the absorption at 885 cm^{-1} (**1**) and 865 cm^{-1} (**2**) in the IR region may correspond to the stretching vibration of M−O double bonds in $[M_2O_7]^{2-}$ anions (M = Mo, W).

The similarity in the structures of these clusters leads to similar electronic spectra, as shown in Figure 3. The red shifts in the spectra of clusters **1** and **3** are expected, since these species contain one Mo atom instead of one W atom. The first absorption peaks of these four clusters located at 424 nm ($3.8\cdot10^3$ $cm^{-1}\cdot mol^{-1}\cdot dm^3$) (**1**), 392 nm ($6.1\cdot10^3$ $cm^{-1}\cdot mol^{-1}\cdot dm^3$) (**2**) and 407 nm ($3.1\cdot10^3$ $cm^{-1}\cdot mol^{-1}\cdot dm^3$) (**3**), 376 nm ($3.9\cdot10^3$ $cm^{-1}\cdot mol^{-1}\cdot dm^3$) (**4**) can be assigned to charge-transfer bands of the type $(\pi)S\rightarrow(d)M$ (M = Mo, W) arising from the MOS_3 moiety. The charge-transfer bands of **1** and **3** are blue-shifted, while those of **2** and **4** are red-shifted compared to those of the free $[MOS_3]^{2-}$ anion (459 nm for Mo and 375 nm for W,

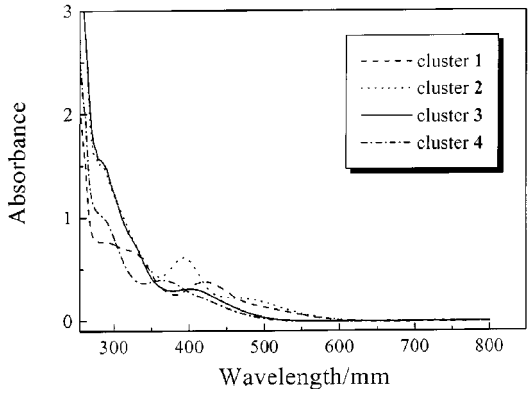

Figure 3. Electronic spectra of $1.0\cdot10^{-4}$ mol·dm^{-3} MeCN solutions of clusters **1**−**4** with an optical pathlength of 1 cm

respectively).[22] The electronic spectra of these four clusters show relatively low linear absorption in the visible and near-infrared regions, promising low intensity loss, and little temperature change caused by photon absorption when pulsed light propagates in the materials, showing that the clusters have potential as optical limiters.

Nonlinear Optical Properties

The third-order nonlinear optical (NLO) properties and the optical limiting (OL) performances of clusters **1**−**4** in MeCN solution were investigated with an 8-ns duration incident pulsed laser at 532 nm. The nonlinear absorption components of clusters **1**−**4** were evaluated by *Z*-scan experiments with an open-aperture configuration (Figure 4). The NLO absorption data obtained under the conditions used in this study can be adequately described by Equations (1) and (2),[23] which describe a third-order NLO absorptive process:

$$T(Z)=\frac{1}{\sqrt{\pi}\,q(Z)}\int_{-\infty}^{+\infty}\ln[1+q(Z)e^{-\tau^2}]\,d\tau \qquad (1)$$

$$q(Z)=\int_{0}^{+\infty}\int_{0}^{+\infty}\alpha_2\frac{I_0}{1+(Z/Z_0)^2}e^{[-2(r/\varpi_0)^2-(t/t_0)^2]}\;\frac{1-e^{-\alpha_0 L}}{\alpha_0}r\,dr\,dt \qquad (2)$$

Here, α_0 and α_2 are linear and effective third-order NLO absorptive coefficients, light transmittance T is a function of the sample's Z-position (with respect to focal point Z = 0), Z is the distance of the sample from the focal point, L is the sample thickness, I_0 is the peak irradiation intensity at focus, $Z_0 = \pi\omega_0^2/\lambda$, where ω_0 is the spot radius of the laser pulse at focus and λ is the laser wavelength, r is the radial coordinate, t is the time, and t_0 is the pulse width.

The nonlinear refractive properties of clusters **1**−**4** were assessed by dividing the normalized Z-scan data obtained under the closed-aperture configuration by the normalized Z-scan data obtained under the open-aperture configuration (Figure 5). An effective third-order nonlinear refractive index n_2 can be derived from the difference between normalized transmittance values at valley and peak positions ($\Delta T_{v\text{-}p}$) using Equation (3), where I is the incident pulsed light intensity.[24]

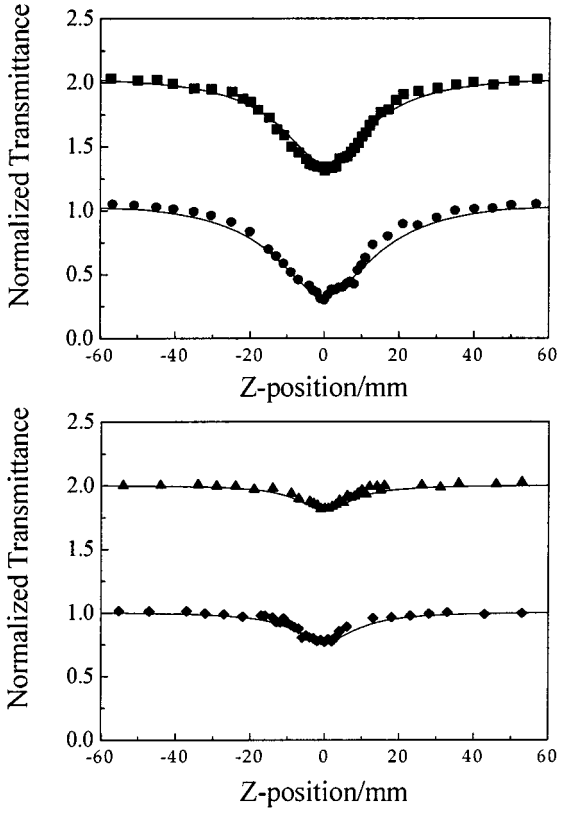

Figure 4. Open-aperture *Z*-scan data of clusters **1** (filled squares), **2** (filled circles), **3** (filled triangles), and **4** (filled diamonds) in MeCN solution at 532 nm with 8 ns wide laser pulses; the solid curves are the theoretical fits based on *Z*-scan theoretical calculations; the *Z*-scan data of both **1** and **3** have been shifted vertically by 1 unit for presentation purposes

$$n_2=\frac{\lambda\alpha_0}{0.812\,\pi I(1-e^{-\alpha_0 L})}\Delta T_{V-P} \qquad (3)$$

Based on our previous time-resolved nonlinear transmission studies[14a] and the NLO experimental results reported here, we can reasonably conclude that the physical origin of the observed reverse saturable absorption (RSA) in clusters **1**−**4** can be attributed to excited-state absorptive nonlinearities. Figures 4 and 5 show the typical NLO absorptive and refractive effects, respectively, of clusters **1**−**4**, in which the filled squares **1**, circles **2**, triangles **3**, and diamonds **4** represent the experimental data from the *Z*-scan measurements, while the solid lines represent the theoretical fitting on the basis of Equations (1)−(3) to the experimental data. A reasonably good fit between the experimental data and theoretical curves was obtained, which suggests that the experimentally obtained NLO effects are effectively third-order in nature. The effective α_2 values of $1.1\cdot10^{-9}$ m·W^{-1} (**1**), $1.2\cdot10^{-9}$ m·W^{-1} (**2**), $5.8\cdot10^{-10}$ m·W^{-1} (**3**), $6.3\cdot10^{-10}$ m·W^{-1} (**4**), and n_2 values of $1.22\cdot10^{-8}$ esu (esu = $7.162\cdot10^{13}$ m^5·v^{-2}) (**1**), $7.18\cdot10^{-9}$ esu (**2**), $6.52\cdot10^{-9}$ esu (**3**), and $5.93\cdot10^{-10}$ esu (**4**), were derived for the samples from

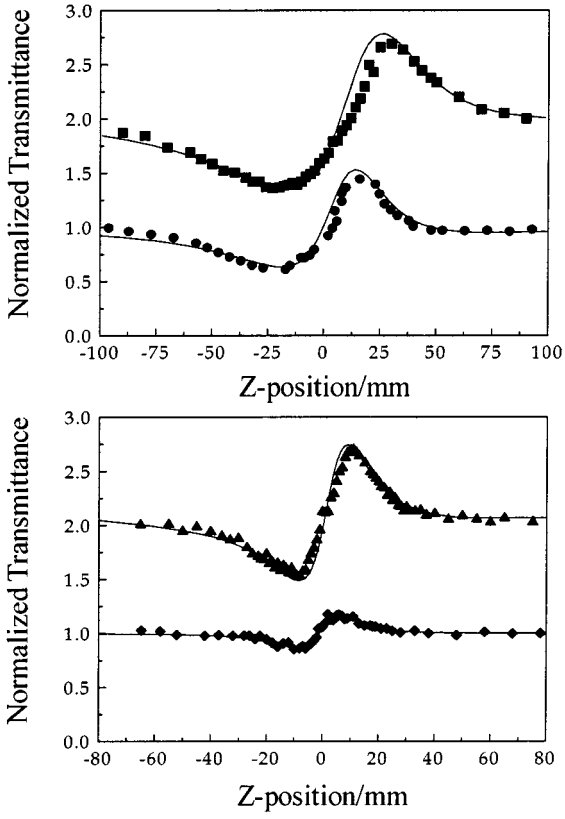

Figure 5. Closed-aperture *Z*-scan data of clusters **1** (filled squares), **2** (filled circles), **3** (filled triangles), and **4** (filled diamonds) in MeCN solution at 532 nm with 8 ns wide laser pulses; the solid curves are the theoretical fits based on *Z*-scan theoretical calculations; the *Z*-scan data of both **1** and **3** have been shifted vertically by 1 unit for presentation purposes

their respective theoretical curves. In accordance with the observed α_2 and n_2 values, the modulus of the effective third-order susceptibility $\chi^{(3)}$ can be calculated by Equation (4).[23a]

$$|\chi^{(3)}| = \sqrt{\left(\left|\frac{9\times10^{8}\varepsilon_0 n_0^2 c^2}{2\nu}\alpha_2\right|^2 + \left|\frac{cn_0^2}{80\pi}n_2\right|^2\right)} \quad (4)$$

Here, ν is frequency of the laser light, n_0 is the linear refractive index of the sample, and ε_0 and c are the permittivity and the speed of light in a vacuum, respectively. For $3.52\cdot10^{-4}$ (**1**), $2.67\cdot10^{-4}$ (**2**), $4.82\cdot10^{-4}$ (**3**), and $3.75\cdot10^{-4}$ mol·dm^{-3} (**4**) MeCN solutions, the $\chi^{(3)}$ values were calculated to be $8.7\cdot10^{-10}$ (**1**), $9.3\cdot10^{-10}$ (**2**), $2.6\cdot10^{-10}$ (**3**), and $3.1\cdot10^{-10}$ esu (**4**). The corresponding moduli of the hyperpolarizabilities γ of $1.32\cdot10^{-30}$ esu (**1**) and $1.87\cdot10^{-30}$ esu (**2**), $2.89\cdot10^{-31}$ esu (**3**) and $4.43\cdot10^{-31}$ esu (**4**), were separately obtained from $\chi^{(3)} = \gamma\cdot NF^4$, where N is the number density (concentration) of the clusters in the samples and $F^4 = 3.1$ is the local field correction factor.

From the above discussions, we can reasonably state that clusters **1**−**4** exhibit similar NLO properties. All exhibit strong RSA and effective self-focusing performances, as depicted in Figures 4 and 5. In the light of the aforementioned nonlinear absorptive and refractive experimental data, an obvious skeleton atom effect on the nonlinear optical properties was observed. For clusters **1**, **2** and **3**, **4**, a significant improvement in the NLO absorptive effects was observed on going from Mo-containing cluster **1** to W-containing cluster **2**, and from cluster **3** to cluster **4**, respectively, i.e. with increasing size of metal atom; this is indicative of a heavy atom effect. On the other hand, although the clusters **1**−**4** possess the same cationic cluster skeleton, their different anions, especially the polyoxometalate anions in clusters **1** and **2**, result in stronger nonlinear absorptive performances and larger $\chi^{(3)}$ values being observed for clusters **1** and **2** as compared to those of clusters **3** and **4**, which demonstrates the evident skeleton influence on the NLO properties of clusters **1**−**4**.

The presence of the combined effects of strong RSA and self-focusing in clusters **1**−**4** may significantly enhance the overall optical limiting (OL) performance of these four clusters. The optical limiting effects of clusters **1**−**4** are depicted in Figure 6. The linear and nonlinear transmission data (open triangles for **1**, filled squares for **2**, open circles for **3**, and filled diamonds for **4**) were measured with 532 nm laser pulses of 8-ns duration at cluster concentrations of $3.52\cdot10^{-4}$ (**1**), $2.67\cdot10^{-4}$ (**2**), $4.82\cdot10^{-4}$ (**3**), and $3.75\cdot10^{-4}$ mol·dm^{-3} (**4**) in MeCN solution. Figure 6 shows how the transmittances of the cluster sample solutions decrease as the laser fluence increases, and how the solution becomes increasingly less transparent as the incident fluence rises, characterizing the typical optical limiting effects. Experiments using neat MeCN solvent gave no detectable OL effect. This indicates that solvent contributions are negligible. The values of the limiting threshold, which is defined as the incident fluence at which the actual transmittance falls to 50% of the corresponding linear transmittance, were measured as 0.26 J·cm^{-2} (**1**), 0.20 J·cm^{-2} (**2**), 0.45 J·cm^{-2} (**3**), and 0.34 J·cm^{-2} (**4**), with the same linear transmittance of 72% in each case.

Table 3 lists the heterothiometallic clusters presented here and investigated previously, together with their limiting thresholds, along with data for some other frequently mentioned OL materials. From the perspective of the OL application, the present four clusters having a nest-shaped skeleton are clearly better than the known good optical limiting materials fullerene C_{60}[6b] and cubane-like shaped clusters,[2a,8] while their limiting thresholds are greater than those of phthalocyanine derivatives,[7b] the hexagonal prism-shaped cluster $[Mo_2Ag_4S_8(PPh_3)_4]$,[10b] and some pentanuclear planar "open" shaped clusters $[MS_4Cu_4L_2(py)_6]$,[14] which are among the best optical limiting materials reported to date. Comparison of clusters **1**, **2** and clusters **3**, **4** allows a comparison of Mo- and W-containing systems. The W-containing clusters always seem able to outperform their corresponding Mo-containing counterparts in OL performance at a given wavelength and with similar linear transmittance, just as in this report where the OL effect of **2** is superior to that of **1**, while **4** is better than **3**. This is consistent with the fact that the OL effects of Ag-containing clusters are better than those of their Cu-containing homologues, which may be due to the

Table 3. The limiting thresholds of some OL materials measured at 532 nm with ns laser pulses

Compound	Structure	Solvent	Linear transmission (%)	Limiting Threshold [J cm^{-2}]	ref.
C_{60}	–	toluene	62	1.6	[6b]
$[Bu_4N]_3[WS_4Cu_3Br_4]$	Cubane-like shaped	MeCN	70	1.1	[8a,8b]
$[Bu_4N]_3[WS_4Ag_3Br_4]$	Cubane-like shaped	MeCN	70	0.6	[8a,8b]
$[Bu_4N]_3[MoS_4Ag_3BrI_3]$	Cubane-like shaped	MeCN	70	0.5	[2a]
$[Bu_4N]_3[MoS_4Ag_3Br_4]$	Cubane-like shaped	MeCN	72	0.7	[8b]
$[Bu_4N]_3[MoS_4Ag_3BrCl_3]$	Cubane-like shaped	MeCN	70	0.6	[2a]
$[Et_4N]_4[Mo_2O_2S_6Cu_6Br_2I_4]$	Twin-nest shaped	MeCN	70	2	[12b]
$[MoOS_3Cu_3(PPh_3)_3\{S_2P(OBu)_2\}]$	Open cubane-like shaped	CH_2Cl_2	90	5	[19]
$[MoS_4Ag_3(PPh_3)_3\{S_2P(OBu)_2\}]$	Open cubane-like shaped	CH_2Cl_2	90	0.8	[19]
$[MoOS_3Cu_3(4\text{-pic})_6]\cdot 0.5[Mo_2O_7]$	Nest shaped	MeCN	72	0.26	this work
$[WOS_3Cu_3(4\text{-pic})_6]\cdot 0.5[W_2O_7]$	Nest shaped	MeCN	72	0.20	this work
$[MoOS_3Cu_3(4\text{-pic})_6]\cdot[BF_4]$	Nest shaped	MeCN	72	0.45	this work
$[WOS_3Cu_3(4\text{-pic})_6]\cdot[BF_4]$	Nest shaped	MeCN	72	0.34	this work
$[MoS_4Cu_6I_4(py)_4]_n$	Two-dimensional network polymer	DMSO	–	0.6	[15b]
$\{[Et_4N]_2[MoS_4Cu_4(CN)_4]\}_n$	Three-dimensional framework polymer	DMF	70	0.28	[15a]
$\{[Et_4N]_2[WS_4Cu_4(CN)_4]\}_n$	Three-dimensional framework polymer	DMF	70	0.15	[15a]
Phthalocyanine derivatives	–	toluene	85	0.1	[7b]
$[Mo_2Ag_4S_8(PPh_3)_4]$	Hexagonal-prism shaped	MeCN	92	0.1	[10b]
$[Et_4N]_2[MoS_4Cu_4(SCN)_4(2\text{-pic})_4]$	Planar "open" shaped	DMF	84	0.5	[14a,14b]
$[Et_4N]_2[WS_4Cu_4(SCN)_4(2\text{-pic})_4]$	Planar "open" shaped	DMF	86	0.3	[14a,14b]
$[MoS_4Cu_4Cl_2(py)_6]$	planar "open" shaped	DMF	78	0.15	[14a]
$[WS_4Cu_4Cl_2(py)_6]$	planar "open" shaped	DMF	64	0.10	[14a]
$[MoS_4Cu_4Br_2(py)_6]$	Planar "open" shaped	DMF	72	0.10	[14a]
$[WS_4Cu_4Br_2(py)_6]$	Planar "open" shaped	DMF	72	0.08	[14a]
$[MoS_4Cu_4I_2(py)_6]$	Planar "open" shaped	DMF	72	0.08	[14a]
$[WS_4Cu_4I_2(py)_6]$	Planar "open" shaped	DMF	72	0.07	[14a]

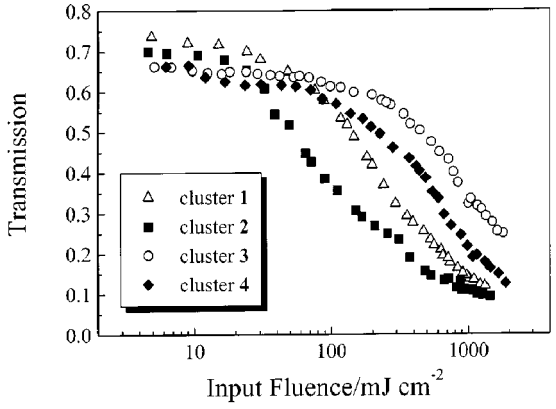

Figure 6. The 8 ns optical limiting effects of clusters **1**–**4** in MeCN solution; the energy transmission is plotted *vs.* the input fluence

heavy-atom effect. The importance of the heavy atom effect with regard to the efficiency of nonlinear absorption and the OL capabilities has already been noted in the case of the metallophthalocyanine system.[7b,25] Moreover, the OL behavior of cluster **1** is greater than that of cluster **3** and the limiting threshold of **2** is superior to that of **4**, which suggests a cluster skeleton effect on their NLO and OL properties. It has been proven that both the cluster skeletons and the heavy atoms are responsible for the NLO effects of the heterothiometallic clusters,[14a] although which one plays a more active and important role in their NLO performances is still not very clear. It currently represents a great challenge and considerable efforts still need to be made to further explore this promising field of research.

Experimental Section

General: All reactions and manipulations were conducted using standard Schlenk techniques under an atmosphere of nitrogen unless specifically mentioned. The compounds $(NH_4)_2[MOS_3]$ (M = Mo, W) were prepared according to the literature.[22] Likewise, the complex $[Cu(MeCN)_4]\cdot[BF_4]$ was synthesized based on a literature procedure.[26] The solvents were carefully dried and distilled prior to use; other chemicals were generally used as received from commercial sources. – Elemental analyses for carbon, hydrogen, and nitrogen were performed on a Perkin–Elmer 240C elemental analyzer. – Infrared spectra were recorded with a Nicolet FT-170SX Fourier transform spectrometer (KBr pellets). – Electronic spectra were measured on a Shimadzu UV-3100 spectrophotometer.

$[MoOS_3Cu_3(4\text{-pic})_6]\cdot 0.5[Mo_2O_7]$ (1): CuCl (0.297 g, 3 mmol) was added to 4-picoline (20 mL) and the solution was stirred for ca. 5 min at room temperature. Then, $(NH_4)_2MoOS_3$ (0.293 g, 1.2 mmol) was added. The reaction mixture immediately turned black-red. After stirring for a further 10 min, the solution was filtered to afford a black-red filtrate. Black-red crystals (0.132 g, 19.8%) were obtained after several days by layering the filtrate with *i*PrOH in air. – $C_{36}H_{42}Cu_3Mo_2N_6O_{4.5}S_3$ (1109.5): calcd. C 39.0, H 3.8, N 7.6; found C 38.7, H 3.9, N 7.8. – UV/vis (MeCN, λ_{max}/nm, 10^3 ε/cm$^{-1}\cdot$mol$^{-1}\cdot$dm^3): 424 (3.8), 326 (6.8), 290 (7.7). – IR (KBr pellets): $\tilde{\nu}$ = 1615 (vs), 1421 (s), 908 (vs), 885 (s), 813 (vs), 492 (vs), 436 (vs).

Table 4. Crystal data for $[MoOS_3Cu_3(4\text{-pic})_6]\cdot 0.5[Mo_2O_7]$ (**1**) and $[WOS_3Cu_3(4\text{-pic})_6]\cdot[BF_4]$ (**4**)

Compound	**1**	**4**
Empirical formula	$C_{36}H_{42}N_6Cu_3Mo_2O_{4.5}S_3$	$C_{36}H_{42}N_6BCu_3F_4OS_3W$
Molecular mass	1109.44	1132.22
Temperature [K]	293(2)	293(2)
Radiation	Mo-K_α (λ = 0.71073 Å)	Mo-K_α (λ = 0.71073 Å)
Crystal color and habit	black-red block	orange-red block
Crystal size [mm]	0.26 × 0.24 × 0.10	0.54 × 0.44 × 0.32
Crystal system	Trigonal	Trigonal
Space group	*P*-3	*P*-3
a [Å]	12.95640(10)	12.6610(18)
b [Å]	12.95640(10)	12.6610(18)
c [Å]	15.26030(10)	15.684(3)
V [Å^3]	2218.51(3)	2177.3(6)
Z	2	2
$D_{calcd.}$ [g·cm^{-3}]	1.661	1.727
F (000)	1110	1116
μ [mm^{-1}]	2.149	4.275
Collection range [°]	$1.33 < \theta < 28.33$	$1.30 < \theta < 25.01$
Scan method	ω scan	ψ scan
Index ranges	$-15 \le h \le 16$ $-17 \le k \le 9$ $-20 \le l \le 18$	$0 \le h \le 15$ $-15 \le k \le 0$ $0 \le l \le 18$
Reflections collected/unique	15712/3640 [R_{int} = 0.0876]	2839/2550 [R_{int} = 0.0847]
Absorption correction	empirical	empirical
Data/restraints/parameters	3640/6/165	2550/8/167
Goodness-of-fit on F^2	1.033	1.073
Final *R* indices [$I > 2\sigma(I)$]	R_1 = 0.0682, wR_2 = 0.2113	R_1 = 0.0563, wR_2 = 0.1542
R indices (all data)	R_1 = 0.1070, wR_2 = 0.2398	R_1 = 0.0769, wR_2 = 0.1640
Largest diff. peak and hole [e·Å^{-3}]	1.340 and −2.776	2.485 and − 2.142

$[WOS_3Cu_3(4\text{-pic})_6]\cdot 0.5[W_2O_7]$ (2): Cluster **2** was synthesized following the same procedure as used in the preparation of cluster **1**, except that $(NH_4)_2WOS_3$ (0.398 g, 1.2 mmol) was used instead of $(NH_4)_2MoOS_3$ (1.2 mmol). Orange-red crystals (0.143 g, 18.5%) were obtained. − $C_{36}H_{42}Cu_3N_6O_{4.5}S_3W_2$ (1285.3): calcd. C 33.6, H 3.3, N 6.5; found C 34.0, H 3.5, N 6.8. − UV/vis (MeCN, λ_{max}/nm, 10^3 ε/cm^{-1}·mol^{-1}·dm^3): 392 (6.1), 283 (15.2). − IR (KBr pellets): $\tilde{\nu}$ = 1615 (vs), 1423 (s), 925 (vs), 865 (s), 813 (vs), 492 (vs), 428 (vs).

$[MoOS_3Cu_3(4\text{-pic})_6]\cdot[BF_4]$ (3): $Cu(MeCN)_4BF_4$ (0.944 g, 3 mmol) was added to 4-picoline (20 mL) and the solution was stirred for ca. 5 min at room temperature. Then, $(NH_4)_2MoOS_3$ (0.244 g, 1 mmol) was added. The reaction mixture immediately turned deep-red. After stirring for a further 10 min, the solution was filtered to afford a deep-red filtrate. Deep-red crystals (0.818 g, 78.3%) were obtained after several days by layering the filtrate with *i*PrOH. − $C_{36}H_{42}BCu_3F_4MoN_6OS_3$ (1044.3): calcd. C 41.4, H 4.1, N 8.1; found C 41.6, H 4.3, N 8.2. − UV/vis (MeCN, λ_{max}/nm, 10^3 ε/cm^{-1}·mol^{-1}·dm^3): 407 (3.1), 281 (15.8). − IR (KBr pellets): $\tilde{\nu}$ = 1614 (vs), 1420 (s), 910 (vs), 813 (vs), 492 (vs), 437 (vs).

$[WOS_3Cu_3(4\text{-pic})_6]\cdot[BF_4]$ (4): Cluster **4** was synthesized following the same procedure as used in the preparation of cluster **3**, except that $(NH_4)_2WOS_3$ (0.332 g, 1 mmol) was used instead of $(NH_4)_2MoOS_3$ (1 mmol). Orange-red crystals (0.965 g, 85.2%) were obtained. − $C_{36}H_{42}BCu_3F_4N_6OS_3W$ (1132.2): calcd. C 38.2, H 3.8, N 7.4; found C 38.3, H 3.9, N 7.5. − UV/vis (MeCN, λ_{max}/nm, 10^3 ε/cm^{-1}·mol^{-1}·dm^3): 376 (3.9), 284 (10.7). − IR (KBr pellets): $\tilde{\nu}$ = 1614 (vs), 1420 (s), 924 (vs), 813 (vs), 492 (vs), 428 (vs).

Crystal Structure Determinations: Well-shaped single crystals of clusters **1** and **4** of suitable dimensions were selected and mounted on glass fibers. The diffraction data for **1** were collected on a Siemens Smart CCD area-detector diffractometer using the ω-scan technique. The data reductions for **1** were performed on a Silicon Graphics Indy workstation using Smart-CCD software. The diffraction data for **4** were collected on an Enraf−Nonius CAD4 four-circle diffractometer with unit-cell parameters determined from the automatic centering of 25 reflections by the least-squares method. Intensities were corrected for Lorentz polarization effects and an absorption correction was applied using the ψ-scan technique. The structures of both **1** and **4** were solved by direct methods and refined by full-matrix least-squares against F^2 using the SHELXL-97 programs.[27] All non-hydrogen atoms were refined anisotropically by the full-matrix least-squares method. The hydrogen atoms were placed in their calculated positions, assigned fixed isotropic thermal parameters, and allowed to ride on their respective parent atoms. The data processing and structure refinement parameters are listed in Table 4.

Crystallographic data (excluding structure factors) for the cluster structures reported in this paper have been deposited with the Cambridge Crystallographic Data Centre as supplementary publications nos. CCDC-164299 (cluster **1**) and CCDC-164300 (cluster **4**). Copies of the data can be obtained free of charge on application to the CCDC, 12 Union Road, Cambridge CB2 1EZ, U.K. [Fax: (internat.) +44 (0)1223/336033; E-mail: deposit@ccdc.cam.ac.uk].

Optical Measurements: A solution of the respective cluster **1**−**4** in MeCN was placed in a 5-mm quartz cuvette for optical limiting

property measurements, which were performed with linearly polarized 8-ns pulses at $\lambda = 532$ nm generated from a Q-switched frequency-doubled Nd:YAG laser. The clusters **1**−**4** proved to be stable towards air and laser light under the experimental conditions. The spatial profiles of the optical pulses were of near-Gaussian transverse mode. The pulsed laser was focused onto the sample cell using a mirror of focal length 30 cm. The spot radius of the laser beam was measured as 55 μm (half-width at $1/e^2$ maximum). The energy of the input and output pulses was measured simultaneously by precision laser detectors (Rjp-735 energy probes), which were linked to a computer through an IEEE interface,[28] while the incident pulse energy was varied by a Newport Com. attenuator. The interval between the laser pulses was chosen as 1 s to avoid the influence of thermal and long-term effects.

The third-order NLO absorptive and refractive properties of clusters **1**−**4** were determined by performing *Z*-scan measurements.[23a] The samples were mounted on a translation stage that was controlled by computer to move along the axis of the incident laser beam (*Z*-direction) with respect to the focal point rather than being positioned at its focal point. To determine both the sign and magnitude of the nonlinear refraction, a 0.2 mm diameter aperture was placed in front of the transmission detector and the transmittance was recorded as a function of the sample position on the *Z* axis (closed-aperture *Z*-scan). To determine the nonlinear absorption, the *Z*-dependent sample transmittance was measured without the aperture (open-aperture *Z*-scan).

Acknowledgments

Dr. C. Zhang greatly appreciates the Alexander von Humboldt Foundation for awarding a Humboldt Research Fellowship. Financial support from the National Science Foundations of China and the USA, the Foundations of the Harbin Institute of Technology and the Universiti Sains Malaysia is acknowledged. C. Z. thanks Scott E. Boesch, Dr. Douglas R. Powell, and Dr. Masood Khan for their helpful discussions.

[1] [1a] E. I. Stiefel, K. Matsumoto, *Transition Metal Sulfur Chemistry: Biological and Industrial Significance*, American Chemical Society, Washington DC, **1996**. – [1b] I. Dance, K. Fisher, *Prog. Inorg. Chem.* **1994**, *41*, 637−803. – [1c] S. C. Lee, R. H. Holm, *Angew. Chem. Int. Ed. Engl.* **1990**, *29*, 840−856.

[2] [2a] S. Shi, W. Ji, S. H Tang, J. P. Lang, X. Q. Xin, *J. Am. Chem. Soc.* **1994**, *116*, 3615−3616. – [2b] S. Shi, Z. R. Chen, H. W. Hou, X. Q. Xin, K. B. Yu, *Chem. Mater.* **1995**, *7*, 1519−1524. – [2c] P. E. Hoggard, H. W. Hou, X. Q. Xin, S. Shi, *Chem. Mater.* **1996**, *8*, 2218−2222. – [2d] S. Shi, W. Ji, X. Q. Xin, *J. Phys. Chem.* **1995**, *99*, 894−898.

[3] [3a] J. B. Howard, D. J. Low, *Chem. Rev.* **1996**, *96*, 2965−2982. – [3b] R. H. Holm, *Adv. Inorg. Chem.* **1992**, *38*, 1−71. – [3c] D. Coucouvanis, *Acc. Chem. Res.* **1991**, *24*, 1−8. – [3d] T. Shibahara, *Coord. Chem. Rev.* **1993**, *123*, 73−147. – [3e] B. C. Wiegand, C. M. Friend, *Chem. Rev.* **1992**, *92*, 491−504.

[4] [4a] A. Muller, E. Diemann, H. Bogge, *Angew. Chem. Int. Ed. Engl.* **1981**, *20*, 934−955. – [4b] C. Zhang, G. C. Jin, J. X. Chen, X. Q. Xin, K. P. Qian, *Coord. Chem. Rev.* **2001**, *213*, 51−77. – [4c] H. W. Hou, X. Q. Xin, S. Shi, *Coord. Chem. Rev.* **1996**, *153*, 25−56. – [4d] S. Sarkar, S. B. S. Mishra, *Coord. Chem. Rev.* **1984**, *59*, 239−264.

[5] [5a] J. Kim, D. C. Rees, *Science* **1992**, *257*, 1677−1682. – [5b] M. K. Chan, J. Kim, D. C. Rees, *Science* **1993**, *260*, 792−794. – [5c] J. T. Bolin, N. Campobasso, S. W. Muchmore, *Molybdenum Enzymes, Cofactors and Model Systems*, American Chemical Society, Washington DC, **1993**.

[6] [6a] L. W. Tutt, A. Kost, *Nature* **1992**, *356*, 225−226. – [6b] D. G. McLean, R. L. Sutherland, M. C. Brant, D. M. Brandelik, P. A. Fleitz, T. Pottenger, *Opt. Lett.* **1993**, *18*, 858−860. – [6c] Y. L. Song, G. Y. Fang, Y. X. Wang, S. T. Liu, C. F. Li, L. C. Song, Y. H. Zhu, Q. M. Hu, *Appl. Phys. Lett.* **1999**, *74*, 332−334. – [6d] Y. P. Sun, J. E. Riggs, *Int. Rev. Phys. Chem.* **1999**, *18*, 43−90.

[7] [7a] J. W. Perry, K. Mansour, I. Y. S. Lee, X. L. Wu, P. V. Bedworth, C. T. Chen, D. Ng, S. R. Mardar, P. Miles, T. Wada, M. Tian, H. Sasabe, *Science* **1996**, *273*, 1533−1536. – [7b] J. W. Perry, K. Mansour, S. R. Marder, K. J. Perry, D. Alvarez Jr., L. Choong, *Opt. Lett.* **1994**, *19*, 625−627. – [7c] C. F. Li, L. Zhang, M. Yang, H. Wang, Y. X. Wang, *Phys. Rev. A* **1994**, *49*, 1149−1157.

[8] [8a] S. Shi, W. Ji, J. P. Lang, X. Q. Xin, *J. Phys. Chem.* **1994**, *98*, 3570−3572. – [8b] W. Ji, H. J. Du, S. H. Tang, S. Shi, *J. Opt. Soc. Am. B* **1995**, *12*, 876−881.

[9] [9a] Z. R. Chen, H. W. Hou, X. Q. Xin, K. B. Yu, S. Shi, *J. Phys. Chem.* **1995**, *99*, 8717−8721. – [9b] H. W. Hou, B. Liang, X. Q. Xin, K. B. Yu, P. Ge, W. Ji, S. Shi, *J. Chem. Soc., Faraday Trans.* **1996**, *92*, 2343−2346.

[10] [10a] G. Salane, T. Shibahara, H. W. Hou, X. Q. Xin, S. Shi, *Inorg. Chem.* **1995**, *34*, 4785−4789. – [10b] W. Ji, S. Shi, H. J. Du, P. Ge, S. H. Tang, X. Q. Xin, *J. Phys. Chem.* **1995**, *99*, 17297−17301. – [10c] T. Xia, A. Dogariu, K. Mansour, D. J. Hagan, A. A. Said, E. W. Van Stryland, S. Shi, *J. Opt. Soc. Am. B* **1998**, *15*, 1497−1501.

[11] [11a] H. W. Hou, X. R. Ye, X. Q. Xin, J. Liu, M. Q. Chen, S. Shi, *Chem. Mater.* **1995**, *7*, 472−476. – [11b] P. Ge, S. H. Tang, W. Ji, S. Shi, H. W. Hou, D. L. Long, X. Q. Xin, S. F. Lu, Q. J. Wu, *J. Phys. Chem. B* **1997**, *101*, 27−31.

[12] [12a] H. W. Hou, D. L. Long, X. Q. Xin, X. Y. Huang, B. S. Kang, P. Ge, W. Ji, S. Shi, *Inorg. Chem.* **1996**, *35*, 5363−5367. – [12b] H. W. Hou, X. Q. Xin, J. Liu, M. Q. Chen, S. Shi, *J. Chem. Soc., Dalton Trans.* **1994**, 3211−3214.

[13] S. Shi, H. W. Hou, X. Q. Xin, *J. Phys. Chem.* **1995**, *99*, 4050−4053.

[14] [14a] C. Zhang, Y. L. Song, B. M. Fung, Z. L. Xue, X. Q. Xin, *Chem. Commun.* **2001**, 843−844. – [14b] C. Zhang, Y. L. Song, G. C. Jin, G. Y. Fang, Y. X. Wang, S. S. S. Raj, H. K. Fun, X. Q. Xin, *J. Chem. Soc., Dalton Trans.* **2000**, 1317−1323.

[15] [15a] C. Zhang, Y. L. Song, Y. Xu, H. K. Fun, G. Y. Fang, Y. X. Wang, X. Q. Xin, *J. Chem. Soc., Dalton Trans.* **2000**, 2823−2829. – [15b] H. W. Hou, Y. T. Fan, C. X. Du, Y. Zhu, W. L. Wang, X. Q. Xin, M. K. M. Low, W. Ji, H. G. Ang, *Chem. Commun.* **1999**, 647−648.

[16] [16a] J. C. Dyason, L. M. Englehardt, P. C. Healy, C. Pakawatchai, A. H. White, *Inorg. Chem.* **1985**, *24*, 1950−1957. – [16b] J. C. Dyason, P. C. Healy, C. Pakawatchai, V. A. Patrick, A. H. White, *Inorg. Chem.* **1985**, *24*, 1957−1960. – [16c] E. W. Ainscough, A. G. Bingham, A. M. Brodie, K. L. Brown, *J. Chem. Soc., Dalton Trans.* **1984**, 989−991.

[17] [17a] H. Yu, W. J. Zhang, X. T. Wu, T. L. Sheng, Q. M. Wang, P. Lin, *Angew. Chem. Int. Ed.* **1998**, *37*, 2520−2521. – [17b] Q. Huang, X. T. Wu, J. X. Lu, *Chem. Commun.* **1997**, 703−704. – [17c] Q. Huang, X. T. Wu, Q. M. Wang, T. L. Sheng, J. X. Lu, *Angew. Chem. Int. Ed. Engl.* **1996**, *35*, 868−870. – [17d] Q. Huang, X. T. Wu, J. X. Lu, *Inorg. Chem.* **1996**, *35*, 7445−7447.

[18] A. Muller, U. Schimanski, J. Schimanski, *Inorg. Chim. Acta* **1983**, *76*, L245−L246.

[19] D. L. Long, S. Shi, X. Q. Xin, B. S. Luo, L. R. Chen, X. Y. Huang, B. S. Kang, *J. Chem. Soc., Dalton Trans.* **1996**, 2617−2622.

[20] D. X. Zeng, W. Ji, W. T. Wong, W. Y. Wong, X. Q. Xin, *Inorg. Chim. Acta* **1998**, *279*, 172−177.

[21] V. W. Day, M. F. Fredrich, W. G. Klemperer, W. Shum, *J. Am. Chem. Soc.* **1977**, *99*, 6146−6148.

[22] J. W. McDonald, G. D. Friesen, L. D. Rosenhein, W. E. Newton, *Inorg. Chim. Acta* **1983**, *72*, 205−210.
[23] [23a] M. Sherk-Bahae, A. A. Said, T. H. Wei, D. J. Hagan, E. W. Van Stryland, *IEEE J. Quantum Electron.* **1990**, *26*, 760−769. – [23b] A. A. Said, M. Sherk-Bahae, D. J. Hagan, T. H. Wei, J. Wang, J. Young, E. W. Van Stryland, *J. Opt. Soc. Am. B* **1992**, *9*, 405−414.
[24] M. Sherk-Bahae, A. A. Said, E. W. Van Stryland, *Opt. Lett.* **1989**, *14*, 955−957.
[25] T. H. Wei, D. J. Hagan, M. J. Sence, E. W. Van Stryland, J. W. Perry, D. R. Coulter, *Appl. Phys. B* **1992**, *54*, 46−51.
[26] E. Heckel, German Patent, 1,230,025, *Chem. Abstr.* **1967**, *66*, 46487e.
[27] G. M. Sheldrick, *SHELXL-97*, *Program for Crystal Structure Determination*, University of Göttingen, Germany, **1997**.
[28] M. Sheik-Bahae, D. C. Hutchings, D. J. Hagan, E. W. Van Stryland, *IEEE J. Quantum Electron.* **1991**, *27*, 1296−1309.

Received May 31, 2001
[I01200]